

Formation and decay of resonance state in ${}^9\text{Be}$ and ${}^9\text{B}$ nuclei. Microscopic three-cluster model investigations.

V. S. Vasilevsky*

*Bogolyubov Institute for Theoretical Physics,
Kiev, Ukraine*

K. Katō†

*Reaction Data Centre, Faculty of Science, Hokkaido University,
Sapporo, Japan*

N. Zh. Takibayev‡

*Al-Farabi Kazakh National University,
Almaty, Kazakhstan*

(Dated: November 14, 2018)

We study nature of the low-lying resonance states in mirror nuclei ${}^9\text{Be}$ and ${}^9\text{B}$. Investigations are performed within a three-cluster model. The model makes use of the hyperspherical harmonics, which provides convenient description of three-cluster continuum. The dominant three-cluster configurations $\alpha + \alpha + n$ and $\alpha + \alpha + p$ in ${}^9\text{Be}$ and ${}^9\text{B}$, respectively, are taken into account. Dominant decay channels for all resonance states in ${}^9\text{Be}$ and ${}^9\text{B}$ are explored. Much attention is paid to the controversial $1/2^+$ resonance states in both nuclei. We study effects of the Coulomb interaction on energy and width of three-cluster resonances in the mirror nuclei ${}^9\text{Be}$ and ${}^9\text{B}$. We also search for the Hoyle-analogue state which is a key step for alternative way of ${}^9\text{Be}$ and ${}^9\text{B}$ syntheses in a triple collision of clusters in a stellar environment.

PACS numbers: 24.10.-i, 21.60.Gx

I. INTRODUCTION

The resonance state is one of the challenging problems for theoretical and nuclear physics. There are common features of resonance states, observed in a few- or many-channel systems. However, there are some specific features connected with the ways of excitation or generation of resonance states and also in different ways resonance state decays in nuclear systems. Special attention is attracted by resonance states formed by three interacting clusters, i.e. resonance states embedded in three-cluster continuum. Such resonance states are repeatedly observed in nuclei with well-determined three-cluster structure. These nuclei have a dominant three-cluster configuration, and it means that bound states and many resonance states are lying below and above, respectively, threshold of three-cluster continuum. In other words, bound states and large part of resonance states in three-cluster nuclei are generated by an interaction of three clusters. As examples of such nuclei, we can mention ${}^5\text{H}$, ${}^6\text{He}$ and ${}^6\text{Be}$, ${}^9\text{Be}$ and ${}^9\text{B}$ and many others.

In the present paper, a microscopic three-cluster model is applied to study nature of resonance states in ${}^9\text{Be}$ and ${}^9\text{B}$. Dominant three-cluster configurations $\alpha + \alpha + n$ and $\alpha + \alpha + p$, respectively, are selected to describe the low excitation energy region in these nuclei. The microscopic

model, which was formulated in Ref. [1], makes use of the total basis of oscillator functions to describe inter-cluster motion. The model is called as AM HHB which stands for the Algebraic three-cluster Model with the Hyperspherical Harmonics Basis. The first application of this model to study resonance structure of ${}^9\text{Be}$ and ${}^9\text{B}$ was made in Ref. [2]. Results presented in Ref. [2] were obtained with the Minnesota potential (MP). In present paper we make use of the modified Hasegawa-Nagata potential (MHNP) [3, 4], and we pay much more attention to the $1/2^+$ resonance states, the Coulomb effects on resonance states in mirror nuclei. Besides, we look for the Hoyle analogue states in ${}^9\text{Be}$ and ${}^9\text{B}$.

There are many attempts to study the resonance structure of ${}^9\text{Be}$ and ${}^9\text{B}$ within different methods and models see, for instance, [5–13]. Mainly, these investigations are performed within the cluster model or different variants of the Resonating Group Method. In some cases, determination of resonance parameters is carried out in the framework of models when three-cluster problem is reduced to the many-channel two-body system by representing ${}^9\text{Be}$ (${}^9\text{B}$) as coupled-channel system ${}^8\text{Be}+n$ (${}^8\text{Be}+p$) and ${}^5\text{He}+{}^4\text{He}$ (${}^5\text{Li}+{}^4\text{He}$). Other group of papers take into account that all resonance states in ${}^9\text{Be}$ and ${}^9\text{B}$ belong three-cluster continuum. Position of resonance states and their properties are determined by using the Complex Scaling Methodology or the Hyperspherical Harmonics basis. The latter allows one to incorporate proper boundary conditions for decay of a compound system on three independent clusters, while the former allows one to locate resonance states in continuum of

* vsvasilevsky@gmail.com

† kato-iku@gd6.so-net.ne.jp

‡ takibayev@gmail.com

many-channel and many-cluster systems.

Special attention is attracted by the $1/2^+$ excited states in ${}^9\text{Be}$ and ${}^9\text{B}$. This is stipulated by two factors. First, position of these resonance was obtained at different energies in various experiments. Some experiments claimed that there are no such resonances in ${}^9\text{Be}$ or ${}^9\text{B}$. Second, different theoretical investigations suggested different energy and nature of the $1/2^+$ excited states in ${}^9\text{Be}$ and ${}^9\text{B}$. Some theoretical investigations stressed there is not the $1/2^+$ excited states in ${}^9\text{Be}$ and that resonance peak in reactions of the photodisintegration is associated with a virtual state. Other group of investigations detected the $1/2^+$ excited states in ${}^9\text{Be}$ and ${}^9\text{B}$ as resonance states in two- or three-body continuum. This dispute also encouraged us to perform the present investigations.

We need to mention numerous experimental investigations of ${}^9\text{Be}$ and ${}^9\text{B}$: [14–21] where structure and different processes taking place in these nuclei are investigated.

Our paper is organized in the following way. In Section II we explain key elements of our model. Main results are presented in Section III. There is a detail discussion on nature of $1/2^+$ resonance states in Section IV. In Section V we discuss effects of the Coulomb interaction on energy and width of resonance states in ${}^9\text{Be}$ and ${}^9\text{B}$, and quest for the Hoyle-analog states is presented in Section VI. We close the paper by summarizing the obtained results in Section VII.

II. MODEL FORMULATION

In this section we shortly outline main ideas of the model.

We start with a wave function of a nucleus consisting of three clusters, as a key element of the model formulation. To describe a three-cluster system one has to construct a three-cluster function

$$\Psi_{JM_J} = \sum_{L,S} \hat{\mathcal{A}} \{ [\Phi_1(A_1, s_1) \Phi_2(A_2, s_2)] \Phi_3(A_3, s_3) \}_S \times f_{L,S}^{(J)}(\mathbf{x}, \mathbf{y}) \}_{JM_J} \quad (1)$$

$$\Psi_{JM_J} = \hat{\mathcal{A}} \left\{ \sum_{c=\{K,l_1,l_2;L,S\}} [[\Phi_1(A_1, s_1) \Phi_2(A_2, s_2)] \Phi_3(A_3, s_3)]_S \mathcal{Y}_{K,l_1,l_2;L}(\Omega)]_{JM_J} \psi_{K,l_1,l_2;L,S}(\rho) \right\}, \quad (5)$$

where hyperradial components $\psi_{K,l_1,l_2;L,S}(\rho)$ of the wave function obey an infinite set of integro-differential equations. The last step toward the simplification of numerical solutions of such a system of equations is to expand the hyperradial amplitudes $\{\psi_{K,l_1,l_2;L,S}(\rho)\}$ over a basis of the hyperradial part of oscillator functions in the

and by solving a many-body Schrödinger equation one has to determine inter-cluster wave function $f_{L,S}^{(J)}(\mathbf{x}, \mathbf{y})$ and spectrum of bound state(s) or S -matrix for states of the continuous spectrum. Jacobi vectors \mathbf{x} and \mathbf{y} determine relative position of clusters. Wave functions $\Phi_\alpha(A_\alpha, s_\alpha)$ ($\alpha=1, 2, 3$), describing internal motion of the cluster consisted of A_α nucleons and with the spin s_α , are assumed to be fixed, and they possess some very important features, for instance, they are antisymmetric and translation-invariant ones. Adiabaticity, connected with a fixed form of the wave functions $\Phi_\alpha(A_\alpha, s_\alpha)$, is the main assumption of the method which is well-known as the Resonating Group Method [22]. In fact, the wave function (1) provides a projection operator which reduces the many-particle problem to an effective three-body problem with nonlocal and energy-dependent potential (see detail in Ref. [22]). For amplitudes

$$f_{L,S}^{(J)}(\mathbf{x}, \mathbf{y}) = \sum_{l_1, l_2} f_{l_1, l_2; L, S}^{(J)}(x, y) \{ Y_{l_1}(\hat{\mathbf{x}}) Y_{l_2}(\hat{\mathbf{y}}) \}_{LM_L} \quad (2)$$

one can deduce an infinite set of the two-dimension (with respect to variables x and y) integro-differential equations. This set of equations can be more simplified. If we introduce hyperspherical coordinates

$$\begin{aligned} x &= \rho \cos \theta, & y &= \rho \sin \theta, \\ \Omega &= \{ \theta, \hat{\mathbf{x}}, \hat{\mathbf{y}} \} \end{aligned} \quad (3)$$

and construct a full set of orthonormal hyperspherical harmonics

$$\mathcal{Y}_{K,l_1,l_2,LM_L}(\Omega) = \chi_{K,l_1,l_2}(\theta) \{ Y_{l_1}(\hat{\mathbf{x}}) Y_{l_2}(\hat{\mathbf{y}}) \}_{LM_L} \quad (4)$$

(see definition of the hyperspherical harmonics, for instance, in [1, 23]), then the wave function (1) is represented as

six-dimension space as

$$\psi_{K,l_1,l_2;L,S}(\rho) = \sum_{n_\rho} C_{n_\rho K, l_1, l_2; L, S}(b) R_{n_\rho, K}(\rho, b), \quad (6)$$

where $R_{n_\rho, K}(\rho, b)$ is an oscillator function

$$R_{n_\rho, K}(\rho, b) = (-1)^{n_\rho} \mathcal{N}_{n_\rho, K} r^K \exp\left\{-\frac{1}{2}r^2\right\} L_{n_\rho}^{K+3}(r^2), \quad (7)$$

$$r = \rho/b, \quad \mathcal{N}_{n_\rho, K} = b^{-3} \sqrt{\frac{2\Gamma(n_\rho + 1)}{\Gamma(n_\rho + K + 3)}},$$

and b is the oscillator length.

Expansion over the oscillator basis reduces the set of integro-differential equations to the system of linear algebraic equations for expansion coefficients

$$\sum_{\tilde{n}_\rho, \tilde{c}} \left\{ \langle n_\rho, c | \hat{H} | \tilde{n}_\rho, \tilde{c} \rangle - E \langle n_\rho, c | \tilde{n}_\rho, \tilde{c} \rangle \right\} C_{\tilde{n}_\rho, \tilde{c}} = 0, \quad (8)$$

where the multiple index c denotes a channel of the hyperspherical basis $c = \{K, l_1, l_2, L, S\}$. This system is relevant to bound states and to continuous spectrum states. To obtain spectrum of bound states, one can use diagonalization procedure for the reduced set of the equations (8). However, to find wave functions and elements of the scattering S -matrix, one has to implement proper boundary conditions for expansion coefficients in Eq. (8). These conditions were thoroughly discussed in Ref. [1].

Completeness relations for hyperspherical harmonics and oscillator functions are

$$\sum_{K, l_1, l_2, LM} \mathcal{Y}_{K, l_1, l_2, LM}(\Omega) \mathcal{Y}_{K, l_1, l_2, LM}(\tilde{\Omega}) = \delta(\Omega - \tilde{\Omega}),$$

$$\sum_{n_\rho} R_{n_\rho, K}(\rho, b) R_{n_\rho, K}(\tilde{\rho}, b) = \delta(\rho - \tilde{\rho}),$$

where delta function $\delta(\Omega - \tilde{\Omega})$ stands for product of five delta functions for each of hyperspherical angles $\{\theta, \hat{\mathbf{x}}, \hat{\mathbf{y}}\} = \{\theta, \theta_{\mathbf{x}}, \varphi_{\mathbf{x}}, \theta_{\mathbf{y}}, \varphi_{\mathbf{y}}\}$. The completeness relations insure us that up to now we made no restrictions or approximations. Approximations will be formulated later, when we proceed to numerical solutions of the system of equations (8).

Note that hyperspherical angles determine the shape and orientation in the space of a triangle connecting the centers of mass of interacting clusters. And thus, the hyperspherical harmonics describe all possible rotations and all possible deformations of the triangle. Each hyperspherical harmonic $\mathcal{Y}_{K, l_1, l_2, LM}(\Omega)$ (similar to the solid harmonics) predetermines one or several dominant shapes of the three-cluster triangles (see some illustrations for this statement in Ref. [24, 25]).

As for functions $\psi_{K, l_1, l_2; L, S}(\rho)$ and $R_{n_\rho, K}(\rho, b)$, they describe radial excitations or monopole or breathing mode excitations. Besides, the wave functions $\psi_{K, l_1, l_2; L, S}(\rho)$ describes all elastic and inelastic processes in three-cluster continuum and thus they contain elements of the scattering S -matrix:

$$\psi_{K, l_1, l_2; L, S}(\rho) \Rightarrow \delta_{c_0, c} \psi_c^{(-)}(k\rho, \eta_c) - S_{c_0, c} \psi_c^{(+)}(k\rho, \eta_c), \quad (9)$$

where c_0 and c denote incoming and present or outgoing channels, respectively; in general case they consist of five quantum numbers $c = \{K, l_1, l_2, L, S\}$. Six dimension incoming $\psi_c^{(-)}(k\rho, \eta_c)$ and outgoing $\psi_c^{(+)}(k\rho, \eta_c)$ waves are determined as follows

$$\psi_c^{(\pm)}(k\rho, \eta_c) = W_{\pm i\eta_c, K+2}(2ik\rho) / \rho^{5/2}, \quad (10)$$

where $W_{\nu, \mu}(z)$ is the Whittaker function (see chapter 13 of book [26]) and η_c is the Sommerfeld parameter

$$\eta_c = \frac{m Z_{c,c} e^2}{\hbar^2 k}.$$

The wave functions $\psi_c^{(\pm)}(k\rho, \eta_c)$ are solutions to the differential equations

$$\left\{ -\frac{\hbar^2}{2m} \left[\frac{d^2}{d\rho^2} + \frac{5}{\rho} \frac{d}{d\rho} - \frac{K(K+3)}{\rho^2} \right] + \frac{Z_{c,c} e^2}{\rho} - E \right\} \psi_c^{(\pm)}(k\rho, \eta_c) = 0, \quad (11)$$

where $Z_{c,c} e^2 / \rho$ represents the effective Coulomb interaction in hyperspherical coordinates. It should be stressed that equation (11) and the Coulomb interaction in this equation represent an asymptotic form of the microscopic three-cluster hamiltonian when distances between interacting clusters are large. The effective charge $Z_{c,c}$ was determined in Ref. [1] and there was suggested an algorithm for its calculation. One can find in Refs. [24] and [27] the explicit values of the effective charge for ${}^6\text{Be}$ and ${}^{12}\text{C}$, respectively.

The asymptotic of wave functions presented in eq. (9) is formulated for the so-called 3-to-3 scattering. This approximation is valid when there are no bound states in any two-cluster subsystem. That is the case for nuclei ${}^9\text{Be}$ and ${}^9\text{B}$ we are going to study.

By closing this section we consider possible values of quantum numbers of the hyperspherical harmonics. First we consider possible values of the partial angular orbital momenta l_1 and l_2 . They determine the total parity of a three-cluster state $\pi = (-1)^{l_1+l_2}$. This implies the first restriction on possible values of l_1 and l_2 . Next, the total orbital momentum L is a vector sum of partial angular orbital momenta l_1 and l_2 : $\mathbf{L} = \mathbf{l}_1 + \mathbf{l}_2$ and thus

$$L = |l_1 - l_2|, |l_1 - l_2| + 1, \dots, l_1 + l_2,$$

and we have got the second restriction. the last restriction is connected with peculiarities of the hyperspherical harmonics. For a fixed value of the hypermomentum K , sum $l_1 + l_2$ can have the following values

$$l_1 + l_2 = K_{\min}, K_{\min} + 2, \dots, K,$$

where $K_{\min} = L$ for the normal parity state $\pi = (-1)^L$ and $K_{\min} = L + 1$ for the abnormal parity state $\pi = (-1)^{L+1}$. Combing the first and third restrictions, we

conclude that the hyperspherical harmonics with even values of K describes positive parity states, while harmonics with odd values of K describes only negative parity states.

Let us consider a partial case of positive parity states with zero value of the total orbital momentum L . In this case the partial orbital momenta $l_1 = l_2 = 0, 1, \dots, K/2$, and for the selected value of the hypermomentum K we have got $K/2 + 1$ hyperspherical functions. If we take all hyperspherical harmonics with $K=0, 2, \dots, K_{\max}$, we will involve $N_{ch} = (K_{\max} + 2)(K_{\max} + 4)/8$ channels in our calculations, where N_{ch} is the number of possible channels c . For an arbitrary value of the total orbital momentum L , by taking into account all hyperspherical harmonics with $K = K_{\min}, K_{\min} + 2, \dots, K_{\max}$, we will involve $N_{ch} = (K_{\max} - K_{\min} + 2)(K_{\max} - K_{\min} + 4)(L + 1)/8$ channels.

As we deal with the oscillator functions, describing three-cluster system, in the following we will use the quantum number N_{sh} which numerates oscillator shells for a state of the compound system with the parity π and the total angular momentum L . An oscillator function $|n_\rho, c\rangle$ with a given values of n_ρ and K belongs to the oscillator shell

$$N_{sh} = n_\rho + (K - K_{\min})/2$$

provided that $K \geq K_{\min}$. This condition means that when $n_\rho = 0$, the oscillator function with hypermomentum $K = K_{\min}$ appears on the oscillator shell $N_{sh} = 0$, and the oscillator function with $K = K_{\min} + 2$ appears on the oscillator shell $N_{sh} = 1$ and so on. If $K = K_{\min}$, then the number of the oscillator shell N_{sh} coincides with the number of the hyperradial excitations n_ρ . On the oscillator shells $N_{sh} \geq (K_{\max} - K_{\min})/2$ we have got a fixed number of the oscillator functions $N_f = (K_{\max} - K_{\min})/2 + 1$.

III. SPECTRUM OF RESONANCE STATES IN ${}^9\text{Be}$ AND ${}^9\text{B}$

To perform numerical calculations, we need to fix a few parameters and select the nucleon-nucleon potential. We start with selection of the nucleon-nucleon potential. We exploit the Modified Hasegawa-Nagata potential (MHNP) [3, 4] to model nucleon-nucleon interaction. This is a semi-realistic potential constructed from the realistic nuclear force by using the reaction matrix method, and it has been intensively used in numerous many-cluster systems, as it provides a good description of the internal structure of clusters and interaction between clusters as well. After the NN potential was selected, we need to fix four input parameters: oscillator length b , number of channels or number of hyperspherical harmonics and number of hyper radial excitations.

We restrict ourselves with a finite set of the hyperspherical harmonics, which is determined by the maximal

TABLE I. Number of channels involved in calculations for different states J^π of ${}^9\text{Be}$ and ${}^9\text{B}$. $N_{ch}(J_-)$ and $N_{ch}(J_+)$ are explained in the text.

J^π	1/2 ⁻	1/2 ⁺	3/2 ⁻	3/2 ⁺	5/2 ⁻	5/2 ⁺	7/2 ⁻	7/2 ⁺	9/2 ⁺
K_{\max}	13	14	13	14	13	14	13	14	14
$N_{ch}(J_-)$	-	21	28	12	21	44	42	30	54
$N_{ch}(J_+)$	29	12	21	44	42	30	30	54	36
N_{ch}	29	33	49	56	63	74	72	84	90

value of the hyperspherical momentum K_{\min} . To describe the positive parity states we use all hyperspherical harmonics with the hypermomentum $K \leq K_{\min} = 14$, the negative parity states are described by the hyperspherical harmonics with $K \leq K_{\min} = 13$. These amounts of the hyperspherical harmonics account for many different scenarios of the three-cluster decay. We also restrict ourselves with number of the hyperradial excitation $n_\rho \leq 100$. This allows us to rich an asymptotic region, where all clusters are well separated and the cluster-cluster interaction, induced by the nucleon-nucleon potential, is negligible small. In Table I we collect information about the number of total channels (N_{ch}) involved in calculations for different values of the total angular momentum J and parity π . We also indicated the number of channels compatible with the total orbital momentum $L = J - 1/2$ ($N_{ch}(J_-)$) and $L = J + 1/2$ ($N_{ch}(J_+)$), naturally $N_{ch} = N_{ch}(J_-) + N_{ch}(J_+)$. Note that the same set of the hyperspherical harmonics was used in Ref. [2].

Since the total spin of nuclei ${}^9\text{Be}$ and ${}^9\text{B}$ equals $S = 1/2$, then the total orbital momentum L is not a quantum number and a state with the total angular momentum J will be presented by a combination of $L = J - 1/2$ and $J = L + 1/2$. One may expect that the spin-orbital forces play a noticeable role in formation of the ground and excited states in ${}^9\text{Be}$ and ${}^9\text{B}$.

We selected a tree of the Jacobi vectors where the first Jacobi vector \mathbf{x} determines distance between center of mass of two alpha particles, while the second Jacobi vector \mathbf{y} indicates a distance of the valence nucleon to the center of mass of two alpha particles. With such a choice of the tree, the partial orbital momentum l_1 of the relative rotation of two alpha particles has only even values. As a consequence of that restriction, the number of independent hyperspherical harmonics is reduced to almost 1/2, and the parity of the compound system is totally determined by the partial orbital momentum l_2 which associated with rotation of the valence nucleon around ${}^8\text{Be}$ as the two-cluster $\alpha + \alpha$ subsystem.

In the present paper, as in previous calculations [2], the oscillator length b is selected to minimize the bound state energy of the alpha particle, which is obtained with $b=1.317$ fm. This allows us to describe correctly the internal structure of the alpha particle. If we take the original form of the MHNP, we obtain the overbounded ground state in ${}^9\text{Be}$ and the bound 3/2⁻ state in ${}^9\text{B}$. The latter contradicts to experiments in ${}^9\text{B}$. The similar situation was observed for the MP. To avoid this unphysical

situation, we changed slightly parameters of the MHNP in order to reproduce bound state energy of ${}^9\text{Be}$. It is necessary to recall, that modification of the Majorana parameter affects only the odd components of the central components of the nucleon-nucleon potential. This modification does not affect the spin-orbital components of the MHNP, which are taken in the original form. Within the present model, the odd components determine the interaction between clusters and are not involved in determining the internal energy of each cluster consisting of s -wave configurations. Thus, by modifying the Majorana parameter, we obtain the correct value of the binding energy of ${}^9\text{Be}$. This is achieved with $m=0.4389$, which can be compared to the original value $m=0.4057$. With this value of the Majorana parameter, the spectrum of resonance states in ${}^9\text{Be}$ and ${}^9\text{B}$ is calculated. In Table II we compare original and new parameters of the MHNP. They are presented in the form

$$V_{2S+1,2T+1}(r) = \sum_{n=1}^3 V_{2S+1,2T+1}^{(n)} \exp\left\{-\frac{r^2}{a_n^2}\right\},$$

where S and T are the spin and isospin of two nucleon system, respectively. One can see that modification of the Majorana parameter changes only the odd components of the intermediate-range in the MHNP.

TABLE II. Original and new parameters of the MHNP. Intensities of the potentials V_{31} , V_{13} , V_{33} , V_{31} , are given in MeV and range of Gaussians a is in fm.

Parameters	Original			New		
	1	2	3	1	2	3
$V_{31}^{(n)}$	-6.0	-546.0	1655.0	-6.0	-546.0	1655.0
$V_{13}^{(n)}$	-5.0	-360.0	1144.6	-5.0	-360.0	1144.6
$V_{33}^{(n)}$	1.667	-70.0	161.5	1.667	-33.746	161.5
$V_{11}^{(n)}$	15.0	50.0	0.0	15.0	86.254	0.0
a_n	2.500	0.942	0.542	2.500	0.942	0.542

One can also see difference between original (O) and modified (M) odd components V_{33} and V_{11} of the Hasegawa-Nagata potential in Figure 1. Increasing of the Majorana parameter leads to a more repulsive character of the odd components of the potential.

A. Two-cluster subsystems

Before proceeding to resonance states in ${}^9\text{Be}$ and ${}^9\text{B}$, let us consider how the MHNP describes their two-cluster subsystems. By using new and original parameters of the MHNP we calculate the spectrum of resonance states in two-cluster subsystem ${}^8\text{Be}$, ${}^5\text{He}$ and ${}^5\text{Li}$. Results of these calculations are presented in Table III. One can see that the MHNP with original parameters describes better the spectrum of the resonance states in ${}^8\text{Be}$, especially the 2^+ and 4^+ resonance states. However, the NN potential with the original and modified sets of parameters

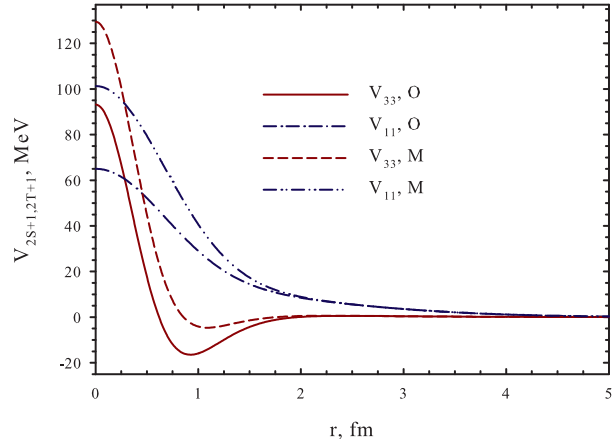


FIG. 1. Odd components of the MHNP as a function of distance between nucleons.

TABLE III. Spectrum of resonance states in ${}^8\text{Be}$, ${}^5\text{He}$ and ${}^5\text{Li}$ calculated with original (O) and modified (M) parameters of the MHNP. Energy E and width Γ are in MeV.

	J^π	O		M		Exp. [28]	
		E	Γ	E	Γ	E	Γ
${}^8\text{Be}$	0^+	0.360	0.032	0.859	0.958	0.092	$5.57 \cdot 10^{-6}$
	2^+	3.196	1.716	4.138	4.809	3.12	1.513
	4^+	11.576	2.569	14.461	6.386	11.44	≈ 3.500
${}^5\text{He}$	$3/2^-$	-0.258	-	0.385	0.209	0.798	0.648
	$1/2^-$	2.307	10.195	2.335	11.927	2.068	5.57
${}^5\text{Li}$	$3/2^-$	0.608	0.162	1.236	0.725	1.69	1.23
	$1/2^-$	3.194	11.986	3.235	13.903	3.18	6.60

yield too wider 0^+ resonance states with a larger energy. The MHNP with the modified Majorana parameter describes better spectrum of resonance states in ${}^5\text{He}$ and ${}^5\text{Li}$ than the this potential with the original value of m . However, theoretical values of energy and width of the lowest resonance states in ${}^5\text{He}$ and ${}^5\text{Li}$ differ noticeable from experimental values. Despite these discrepancies between calculated and experimental spectrum of resonance states in two-cluster systems ${}^8\text{Be}$, ${}^5\text{He}$ and ${}^5\text{Li}$, we are going to use the MHNP with the modified value of the parameter m to study spectrum of three-cluster resonance states in compound ${}^9\text{Be}$ and ${}^9\text{B}$ nuclei. As well known (see, for instance, Ref. [2] and references therein), it is impossible to reproduce properly spectrum of ${}^9\text{Be}$ and ${}^9\text{B}$ with the semi-realistic nucleon-nucleon potential, which properly describe structure of two-cluster subsystems ${}^8\text{Be}$, ${}^5\text{He}$ and ${}^5\text{Li}$.

Now we turn our attention to the spectrum of ${}^9\text{Be}$ and ${}^9\text{B}$ nuclei. Results of calculations with the MHNP are presented in Tables IV and V where we compare our results with the experimental data [29]. Results of our calculations are in fairly good agreement with available experimental data. Energy and width of some resonance

states are rather close to experimental data, for instance, parameters of the $5/2^-$ and $9/2^+$ resonance states in ${}^9\text{Be}$, and parameters of the $5/2^-$, $1/2^-$ and $5/2^+$ resonance states in ${}^9\text{B}$.

TABLE IV. Spectrum of bound and resonance states of ${}^9\text{Be}$ calculated with the MHNP.

J^π	Exp.		AM HHB, MHNP	
	$E(\text{MeV}\pm\text{keV})$	$\Gamma(\text{MeV}\pm\text{keV})$	$E(\text{MeV})$	$\Gamma(\text{MeV})$
$3/2^-$	-1.5735		-1.5743	
$1/2^+$	0.111 ± 7	0.217 ± 10	0.338	0.168
$5/2^-$	0.8559 ± 1.3	0.00077 ± 0.15	0.897	$2.363\cdot 10^{-5}$
$1/2^-$	1.21 ± 120	1.080 ± 110	2.866	1.597
$5/2^+$	1.476 ± 9	0.282 ± 11	2.086	0.112
$3/2^+$	3.131 ± 25	0.743 ± 55	4.062	1.224
$3/2_2^-$	4.02 ± 100	1.33 ± 360	2.704	2.534
$7/2^-$	4.81 ± 60	1.21 ± 230	4.766	0.404
$9/2^+$	5.19 ± 60	1.33 ± 90	4.913	1.272
$5/2_2^-$	6.37 ± 80	~ 1.0	5.365	4.384
$7/2^+$			5.791	3.479

TABLE V. Experimental and theoretical spectrum of resonance states of ${}^9\text{B}$.

J^π	Exp.		AM HHB, MHNP	
	$E(\text{MeV}\pm\text{keV})$	$\Gamma(\text{MeV}\pm\text{keV})$	$E(\text{MeV})$	$\Gamma(\text{MeV})$
$3/2^-$	0.277	0.00054 ± 0.21	0.379	$1.076\cdot 10^{-6}$
$1/2^+$	(1.9)	$\simeq 0.7$	0.636	0.477
$5/2^-$	2.638 ± 5	0.081 ± 5	2.805	0.018
$1/2^-$	3.11	3.130 ± 200	3.398	3.428
$5/2^+$	3.065 ± 30	0.550 ± 40	3.670	0.415
$3/2^+$			4.367	3.876
$3/2_2^-$			3.420	3.361
$7/2^-$	7.25 ± 60	2.0 ± 200	6.779	0.896
$9/2^+$			6.503	2.012
$5/2_2^-$	12.670 ± 40	0.45 ± 20	5.697	5.146
$7/2^+$			7.100	4.462

Spectrum of the ground and excited states in ${}^9\text{Be}$ and ${}^9\text{B}$, presented in Figure 2, where spectrum is displayed as a function of $J(J+1)$, shows that there are three rotational bands in these nuclei. They can be marked in the standard manner as $K = 3/2^-$, $K = 1/2^-$, and $K = 1/2^+$ rotational bands. The main $K = 3/2^-$ rotational bands are comprised of the $3/2_1^-$, $5/2_1^-$ and $7/2_1^-$ states and are represented by almost straight lines in both nuclei. It means that the effective moment of inertia is of a rigid-body type, since it is independent of the total angular momentum J . This is the first rotational band for negative parity states. The second negative-parity rotational $K = 1/2^-$ band involves also three states $1/2^-$, $3/2_2^-$ and $5/2_2^-$. A bent line connects these states. However, that part of line which connects $3/2_2^-$ and $5/2_2^-$ states, is parallel to the line of the first rotational band. Such shape of a line in the $K = 1/2^-$ band indicates that the Coriolis forces are strong in the $1/2^-$ state and are very small in the $3/2_2^-$ and $5/2_2^-$ states. The Coriolis forces,

associated with the interaction of the internal and collective degrees of freedom, are rather strong in the states of the positive parity rotational $K = 1/2^+$ band. Especially they are very strong for the $3/2^+$ and $9/2^+$ states, since these states strongly bends a line collecting states of this band. As in the case of the $K = 1/2^-$ band, the line connecting the $5/2^+$ and $7/2^+$ is also parallel to the line of the first rotational $K = 3/2^-$ band. It is interesting to note a close similarity in the structure of rotational bands in ${}^9\text{Be}$ and ${}^9\text{B}$ nuclei.

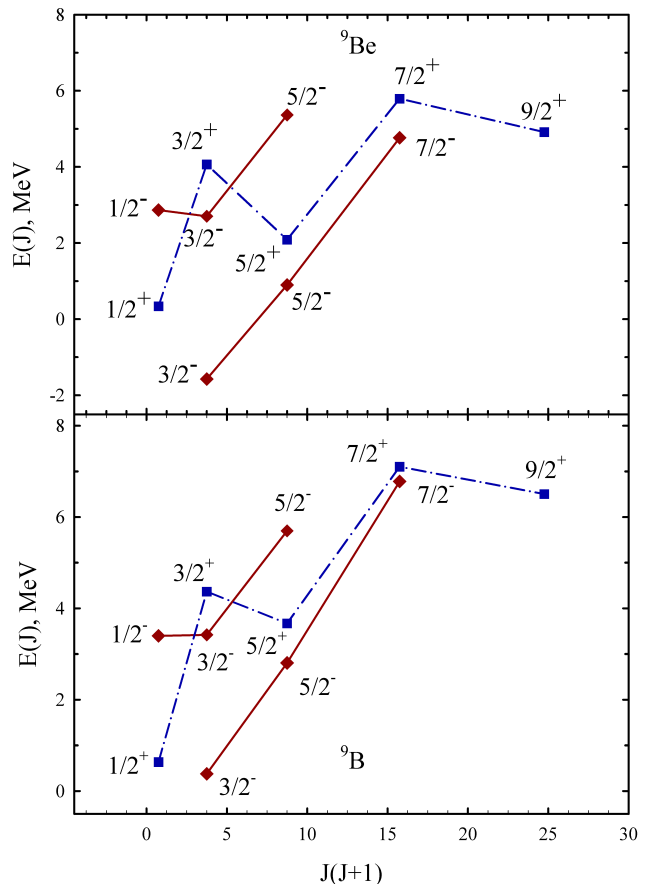


FIG. 2. Spectrum of rotational bands in ${}^9\text{Be}$ and ${}^9\text{B}$.

In Figures 3 and 4 we compare results of our present calculations (MHNP), with results of previous investigations (MP), presented in [2], and with available experimental data [29].

There are two main differences between previous calculations with the MP and new ones with the MHNP. First, the MHNP generates much less (approximately two times) of resonance states within the considered region of energy. Second, the MHNP does not create many narrow resonance states. The common feature of these two calculations is that the $1/2^+$ resonance states in ${}^9\text{B}$ and ${}^9\text{Be}$ are observed close to the three-cluster threshold $\alpha+\alpha+N$. It is worth to recall, that parameters of the MP

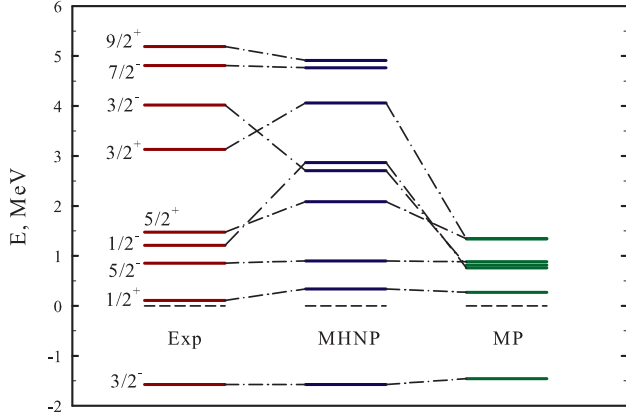


FIG. 3. Experimental (Exp) and calculated spectrum of ${}^9\text{Be}$ determined with the MHNP and MP.

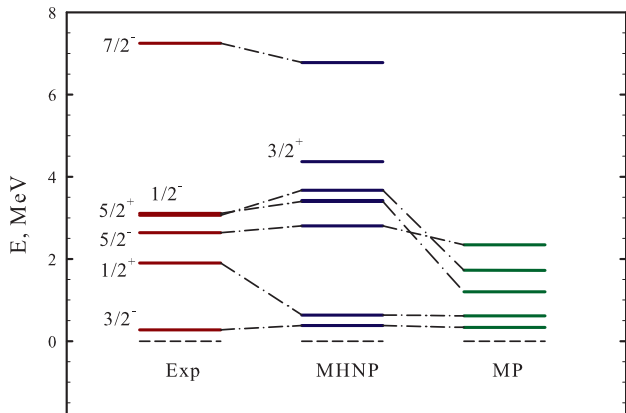


FIG. 4. Experimental and calculated spectrum of ${}^9\text{B}$.

and MHNP potentials were adjusted to reproduce energy of the $3/2^-$ ground state in ${}^9\text{Be}$. With these parameters we obtained the $3/2^-$ resonance states of ${}^9\text{B}$ at the energy very close to the experiment. This result means that we found the correct interaction between clusters in ${}^9\text{B}$ and ${}^9\text{Be}$. In this paper, as in the previous one [2], we use the same parameters of nucleon-nucleon interactions for all other J^π states. From Figures 3 and 4 we conclude that the MHNP generates more correct cluster-cluster interaction for many sets of the J^π states, than the MP. We also conclude that spectrum of resonance states in ${}^9\text{B}$ and ${}^9\text{Be}$ strongly depends on peculiarities of the nucleon-nucleon interaction.

In Figure 5 we provide more detail comparison of some resonance states calculated with the MHNP and MP. As we see position of selected resonance states (namely $5/2^-$ and $1/2^+$ in both nuclei, and $3/2^-$ in ${}^9\text{B}$) are almost in-

dependent or slightly dependent on the shape of nucleon-nucleon potentials.

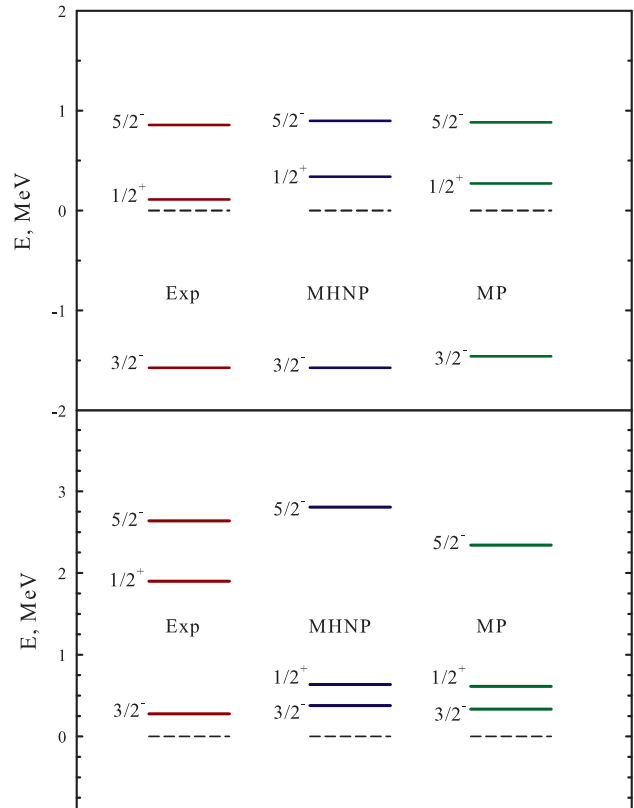


FIG. 5. Comparison of some resonance states in ${}^9\text{Be}$ and ${}^9\text{B}$ calculated with the MHNP and MP potentials and with experimental data.

IV. PROPERTIES OF THE $1/2^+$ RESONANCES STATES

A. Resonance solutions in the hyperspherical harmonics method

Now we turn our attention to the $1/2^+$ resonance states in ${}^9\text{B}$ and ${}^9\text{Be}$. In this section we are going to present more details about calculations of resonance states within the present model. Numerical solutions of the dynamic equations (8) give us $N_{ch} \times N_{ch}$ elements of the S-matrix $\|S_{c,\bar{c}}\|$ and set of wave functions for a given value of energy. We analyze the behavior of the diagonal matrix elements $S_{c,c}$ of the S-matrix, which we represent as $S_{c,c} = \eta_{c,c} \exp\{2i\delta_{c,c}\}$, where $\delta_{c,c}$ is the phase shift and $\eta_{c,c}$ is the inelastic parameter. This analysis helps us to reveal resonance states and determine some of their physical properties. However, energy of the resonance state

and its total width are determined by using an uncoupled channel or eigenchannel representation which is obtained by reducing the scattering matrix $\|S_{c,\tilde{c}}\|$ to the diagonal form. Details of such transformations are explained in Ref. [30]. The representation allows us to calculate partial widths, to discover dominant decay channels and thus to shed more light on nature of investigated resonance states.

In Figures 6 and 7 we display the diagonal phase shifts and inelastic parameters of $3\Rightarrow 3$ scattering for the $1/2^+$ state in ${}^9\text{B}$ and ${}^9\text{Be}$, respectively. These results are obtained with $K_{\text{max}}=14$ and with the MHNP. With such a value of K_{max} , 32 channels are involved in calculations (see Table I) and only three of them produces phase shifts which are not very small at the energy region $0 \leq E \leq 5$ MeV. The phase shift connected with the channel $c = \{K = 0, l_1 = 0, l_2 = 0, L = 0\}$ of ${}^9\text{Be}$ shows resonance behavior at energies $E=0.338$ MeV and $E=1.432$ MeV. The second resonance state is also reflected in the second channel $c = \{K = 2, l_1 = 0, l_2 = 0, L = 0\}$ as a shadow resonance. One should to recall, that the shadow resonance appears in many-channel systems when it created in one channel and reflects in other channels. The most famous shadow resonance states are the $3/2^+$ resonance states in ${}^5\text{He}$ and ${}^5\text{Li}$ which were thoroughly discussed in book [22]. These resonance states are created by the Coulomb barrier in $d+t$ and $d+{}^3\text{He}$ channels, respectively, and they also reflected in $\alpha+n$ and $\alpha+p$ channels. If one disconnects $d+t$ and $\alpha+n$ or $d+{}^3\text{He}$ and $\alpha+p$ channels, then one will observe the resonance state only in the first $d+t$ or $d+{}^3\text{He}$ channel. See more detail discussion of the shadow resonance states in Refs. [31, 32].

Phase shifts δ_{cc} for the $1/2^+$ state in ${}^9\text{B}$ also exhibit resonance states at two energies $E=0.636$ MeV and $E=2.875$ MeV. As in the case of ${}^9\text{Be}$, resonance states in $1/2^+$ state of ${}^9\text{B}$ are connected with only one channel

$$c = \{K = 0, l_1 = 0, l_2 = 0, L = 0\}.$$

Due to the Coulomb interaction, resonance states in ${}^9\text{B}$ are shifted to a higher energy region with respect to position of these resonance states in ${}^9\text{Be}$. It is interesting to note that one observes only elastic processes around the first $1/2^+$ resonance state in both nuclei, as the inelastic parameters $\eta_{cc} = 1$. Meanwhile, the elastic and inelastic processes are quite intensive around the second $1/2^+$ resonance state in ${}^9\text{B}$ and ${}^9\text{Be}$. These results mean that only one channel dominates in formation of the first $1/2^+$ resonance state, and that more channels are involved in formation and decay of the second $1/2^+$ resonance states.

Phase shifts δ_{cc} for the $1/2^+$ state in ${}^9\text{Be}$ and ${}^9\text{B}$ demonstrate that the total orbital momentum $L = 0$ dominates in this state. Can we neglect the total orbital momentum $L=1$ to form the $1/2^+$ state? What is role of that value of the total orbital momentum? To answer these questions, we make additional calculations by neglecting the state with $L=1$. In this case we obtain the $1/2^+$ resonance state in ${}^9\text{Be}$ with parameters $E=0.340$

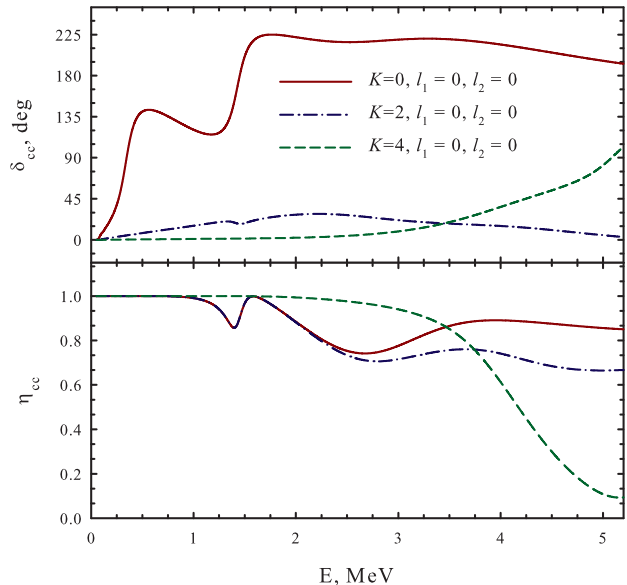


FIG. 6. Phase shifts δ_{cc} and inelastic parameters η_{cc} for the $3\Rightarrow 3$ scattering for the $J^\pi = 1/2^+$ state in ${}^9\text{Be}$.

MeV and $\Gamma=0.171$ MeV which is close to results with $L=0$ and $L=1$: $E = 0.338$ MeV and $\Gamma=0.168$ MeV. In ${}^9\text{B}$ we obtain $E=0.649$ MeV and $\Gamma=0.475$ which has to be compared with $E=0.636$ MeV and $\Gamma=0.477$. Thus, one may obtain quite correct values of energy and total width of the $1/2^+$ resonance state in ${}^9\text{Be}$ and ${}^9\text{B}$ by omitting the state $L=1$.

It is important to note that with the MHNP we obtain the $1/2^+$ resonance state in ${}^9\text{Be}$ and ${}^9\text{B}$ with energy 0.338 and 0.636 MeV, respectively. These energies are smaller than the energy of binary channel thresholds ${}^8\text{Be}+n$ and ${}^8\text{Be}+p$, if we take energy of the 0^+ resonance state as the "ground state" of ${}^8\text{Be}$. As we can see from Table III, this energy equals 0.859 MeV. Thus our model with the MHNP suggests that the $1/2^+$ resonance state in ${}^9\text{Be}$ and ${}^9\text{B}$ is of the three-cluster nature. Let us compare what this model suggested for the MP. Energy of the $1/2^+$ resonance state in ${}^9\text{Be}$ and ${}^9\text{B}$, calculated in Ref. [2] with the MP, equals 0.25 and 0.59 MeV, respectively, which is higher than the energy $E=0.17$ MeV of binary thresholds ${}^8\text{Be}+n$ and ${}^8\text{Be}+p$. Thus the 0^+ resonance state in ${}^8\text{Be}$ may participate in formation of the $1/2^+$ resonance state in ${}^9\text{Be}$ and ${}^9\text{B}$.

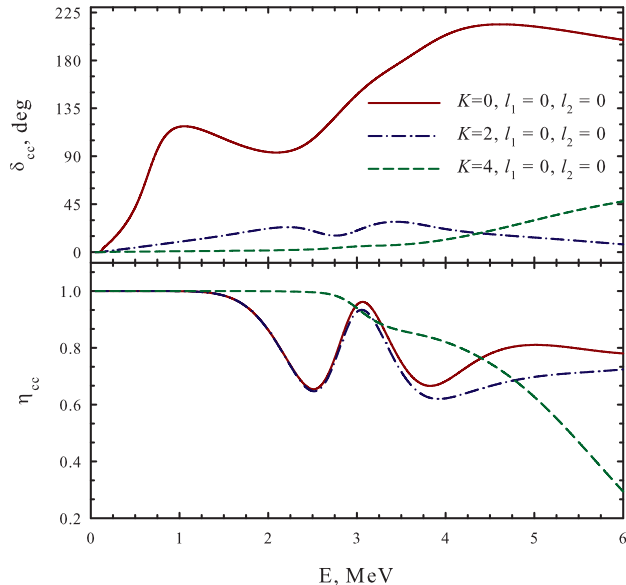


FIG. 7. Phase shifts δ_{cc} and inelastic parameters η_{cc} for the $3 \Rightarrow 3$ scattering for the $J^\pi = 1/2^+$ state in ${}^9\text{B}$.

TABLE VI. Convergence of parameters of the $1/2^+$ resonance state in ${}^9\text{Be}$ and ${}^9\text{B}$.

Nucleus	K_{\max}	4	6	8	10	12	14
${}^9\text{Be}$	E , MeV	0.338	0.338	0.338	0.338	0.338	0.338
	Γ , MeV	0.179	0.175	0.172	0.171	0.169	0.168
	E , MeV	4.972	3.710	2.091	1.886	1.764	1.432
	Γ , MeV	3.827	3.869	1.194	0.641	0.634	0.233
${}^9\text{B}$	E , MeV	0.629	0.631	0.633	0.634	0.636	0.636
	Γ , MeV	0.493	0.487	0.483	0.481	0.479	0.477
	E , MeV		5.173	4.434	3.948	3.030	2.875
	Γ , MeV		3.287	3.001	3.350	1.978	1.235

B. Resonance wave functions in the oscillator shell representation

1. Convergence of resonance energy and width

To demonstrate that we involve a large set of the hyperspherical harmonics, which provides convergent results for energy and width of resonance states, we consider how they depend on number of hyperspherical harmonics. In Table VI we demonstrated convergence of parameters of the $1/2^+$ resonance state in ${}^9\text{B}$ and ${}^9\text{Be}$. As we see, parameters of the first $1/2^+$ resonance state in ${}^9\text{B}$ and ${}^9\text{Be}$ are quite stable when we increase basis of hyperspherical harmonics from $K_{\max} = 4$ to $K_{\max} = 14$. However, it is not the case for the second $1/2^+$ resonance state in ${}^9\text{B}$ and ${}^9\text{Be}$, as more larger set of the hyperspherical harmonics participate in formation of the second resonance state.

TABLE VII. Total Γ and partial widths Γ_i for the second $1/2^+$ resonance states in ${}^9\text{Be}$ and ${}^9\text{B}$.

${}^9\text{Be}$												
$E=1.432$ MeV, $\Gamma=0.2327$ MeV												
i	K	l_1	l_2	L	Γ_i	Γ_i/Γ	K	l_1	l_2	L	Γ_i	Γ_i/Γ
1	0	0	0	0	0.1858	79.82	0	0	0	0	0.1858	79.82
2	2	0	0	0	0.0458	19.67	2	0	0	0	0.0293	12.59
3	4	2	2	0	0.0009	0.39	2	1	1	0	0.0165	7.08
4	4	2	2	1	0.0001	0.08	4	1	1	0	0.0006	0.262
5							4	2	2	0	0.0004	0.17
6							4	2	2	1	0.0001	0.05
Tree	$n + {}^8\text{Be}$						${}^4\text{He} + {}^5\text{He}$					
${}^9\text{B}$												
$E=2.871$ MeV, $\Gamma=1.2355$ MeV												
i	K	l_1	l_2	L	Γ_i	Γ_i/Γ	K	l_1	l_2	L	Γ_i	Γ_i/Γ
1	0	0	0	0	1.1072	89.62	0	0	0	0	1.1072	89.62
2	2	0	0	0	0.1154	9.34	2	0	0	0	0.0739	5.98
3	4	0	0	0	0.0025	0.20	2	1	1	0	0.0416	3.36
4	4	2	2	0	0.0088	0.72	4	1	1	0	0.0084	0.68
5	4	2	2	1	0.0013	0.10	4	2	2	0	0.0030	0.24
6							4	1	1	1	0.0005	0.04
7							4	2	2	1	0.0008	0.07
Tree	$n + {}^8\text{Be}$						${}^4\text{He} + {}^5\text{He}$					

Our method allows to reveal dominant decay channels by calculating partial widths Γ_i ($i=1,2,\dots,N_{ch}$, $\Gamma = \sum_{i=1}^{N_{ch}} \Gamma_i$) of each resonance state. An algorithm for their determination is presented in Ref. [30]. We consider partial widths only of the second $1/2^+$ resonance states in ${}^9\text{Be}$ and ${}^9\text{B}$. In Table VII we present total and partial widths of those channels which make noticeable contribution to the total width of the resonance state. In this Table we also show a ration Γ_i/Γ in percent ($i=1,2,\dots$), which explicitly indicates the most probable decay channels of the considered resonances. Note that the total contribution of the presented channels exceeds 99.95 %.

In Tables VIII and IX we collect different experimental and theoretical results concerning parameters of the $1/2^+$ resonance state in ${}^9\text{Be}$ and ${}^9\text{B}$. Here, ACCCM stands for the analytic continuation in a coupling constant method [33], and GCM means the Generator Coordinate Method [8]. Both methods make use of the same part of the Hilbert space as we use in our model. In Ref. [8] the Volkov potential N2 supplemented with the zero-range spin-orbital interaction represents the nucleon-nucleon interaction, while the MP is involved in the ACCCM calculations [33]. The ACCCM model generates a very broad $1/2^+$ resonance state in both nuclei. Energy of these resonances exceeds 2 MeV. Parameters of the $1/2^+$ resonance states determined within the GCM are close to experimental values especially for ${}^9\text{Be}$. The GCM implies that the $1/2^+$ resonance state in ${}^9\text{B}$ is broad. Within our model we obtain energy of the $1/2^+$ state in ${}^9\text{Be}$ is close to experimental, however, its width is smaller than experimental. The calculated width with the MP is very small. In ${}^9\text{B}$, our model generates two resonance states,

TABLE VIII. Parameters of the $1/2^+$ resonance state in ${}^9\text{Be}$ determined by different experimental and theoretical methods.

${}^9\text{Be}$			
Method	Source	E , MeV	Γ , keV
(e, e')	[34]	1.684 ± 0.007	217 ± 10
(e, e')	[19]	1.68 ± 0.015	200 ± 20
(γ, n)	[17]	1.750 ± 0.010	283 ± 42
(e, e')	[18]	1.732	270
β decay	[35]	1.689 ± 0.010	224 ± 7
(e, e')	[15]	1.748 ± 0.006	274 ± 8
(γ, n)	[36]	1.728 ± 0.001	214 ± 7
ACCCM	[33]	2.52	2620
GCM	[8]	1.55	360
AM HHB, MP	[2]	1.802	15
AM HHB, MHNP	Present	1.912	168

TABLE IX. Parameters of the $1/2^+$ resonance state in ${}^9\text{B}$ determined by different experimental and theoretical methods.

${}^9\text{B}$			
Method	Source	E , MeV	Γ , MeV
Compilation	[16]	1.0	1.8
${}^6\text{Li}({}^6\text{Li}, t)$	[21]	0.73 ± 0.05	≈ 0.3
${}^{10}\text{B}({}^3\text{He}, \alpha)$	[37]	1.8 ± 0.2	0.9 ± 0.3
${}^6\text{Li}({}^6\text{Li}, d)$	[38]	0.8–1.0	≈ 1.5
ACCCM	[33]	2.0	2.7
GCM	[8]	1.27	1.24
AM HHB, MP	[2]	0.30	0.12
AM HHB, MP	[2]	2.08	0.83
AM HHB, MHNP	Present	0.26	0.48
AM HHB, MHNP	Present	2.50	1.24

one of which is close to the "ground state" of the nucleus ($E \approx 0.3$ MeV) and the second one has an excitation energy $E > 2$ MeV and a width around 1 MeV.

2. Wave functions of resonance states

To understand nature of $1/2^+$ resonance states in ${}^9\text{B}$ and ${}^9\text{Be}$, we analyze wave functions. As was mentioned above the wave function of the three-cluster system has many-components and is a huge object which is difficult to analyze. The simplest way for analyzing the wave function of a resonance state is to study weights of oscillator shells. In Fig. 8 we show the weight W_{sh} of different oscillator shell N_{sh} ($N_{sh} = 0, 1, 2, \dots$) in the wave function of resonance states. The weights are determined as follows

$$W_{sh} = W_{sh}(N_{sh}) = \sum_{n_\rho, c \in N_{sh}} |C_{n_\rho, c}|^2.$$

It is important to note that oscillator wave functions with small values of N_{sh} describe very compact configurations of the three-cluster system, when distance between interacting clusters is very small. Oscillator functions with large values of N_{sh} account for configurations of the

three-cluster system with a large distance between all clusters and/or when one cluster is far away from two other clusters. These statements can be deduced from the fact that the radius (or average size) of a three-cluster system, describing by an oscillator function from the N_{sh} oscillator shell, is equal approximately to $b \cdot \sqrt{4N_{sh} + 3}$.

One can see that the wave function of the $1/2^+$ resonance in ${}^9\text{Be}$ is similar to the wave function of the resonance state in ${}^9\text{B}$ and both of them are represented by the oscillator shells with large values of N_{sh} . Figure 8 displays the behavior of the wave function which is typical for low-energy wave functions. In asymptotic region, which is not display here, these functions have an oscillatory behavior. This statement is justified by the following considerations. Like in a two-body case with a sort-range interaction, the position of the first node of the wave function shifts to at larger distances from the origin as the energy decreases to zero. In the oscillator space we have approximately the same picture as it seen in the coordinate space. This is because there is a simple relation between the wave function in the coordinate space and expansion coefficients in the oscillator representation (see detail, for instance, in [1]). To make it clear, we consider a simple case. Suppose that we involve only one channel to describe $1/2^+$ state in ${}^9\text{B}$ and ${}^9\text{Be}$. This channel has zero value of the hypermomentum and thus partial orbital momenta $l_1 = l_2 = 0$ and the total orbital momentum $L=0$. An asymptotic part of the single-channel wave function in the hyperspherical harmonic formalism is [39, 40]

$$\psi_{K=0}(\rho) \approx \frac{\cos(k\rho + \delta_0 - 5\pi/4)}{\rho^{5/2}}, \quad \rho \gg 1,$$

while in the oscillator representation the expansion coefficients are

$$C_{n_\rho K=0}(b) \approx \sqrt{2}R_n^2 \cdot \frac{\cos(kbR_n + \delta_0 - 5\pi/4)}{R_n^{5/2}}, \quad n_\rho \gg 1, \quad (12)$$

where δ_0 is the phase shift of $3 \Rightarrow 3$ scattering with the hypermomentum $K=0$ and

$$R_n = \sqrt{4n_\rho + 6},$$

$$k = \sqrt{\frac{2mE}{\hbar^2}}.$$

For the sake of simplicity we assume that there is no Coulomb interaction in both ${}^9\text{Be}$ and ${}^9\text{B}$ nuclei. Expansion coefficients (12) indicate that the weight of the oscillator shell $N_{sh} = n_\rho$ equals approximately

$$W_{n_\rho} \approx \left| \frac{\cos(kbR_n + \delta_0 - 5\pi/4)}{\sqrt{R_n}} \right|^2 \quad (13)$$

and tends to zero as n_ρ goes to infinity due to the denominator proportional to $n_\rho^{1/2}$. It is seen from (13) that oscillator shells which obey the conditions

$$kbR_n + \delta_0 - 5\pi/4 = \nu\pi/2, \quad \nu = 1, 2, \dots,$$

give a negligibly small contribution to the wave function in the oscillator representation $C_{n_\rho K=0}$ and, consequently, to the weight W_{n_ρ} . One may expect a node of the wave function at this point of the discrete coordinate n_ρ .

In a more complicated case, when a large number of hyperspherical harmonics are involved in calculations, one expect an oscillatory behavior of the wave functions and weights of the oscillator shells W_{sh} for any state of continuous spectrum states. For states with large energies, more nodes of the wave function in the oscillator representation can be observed within the finite range of oscillator shells.

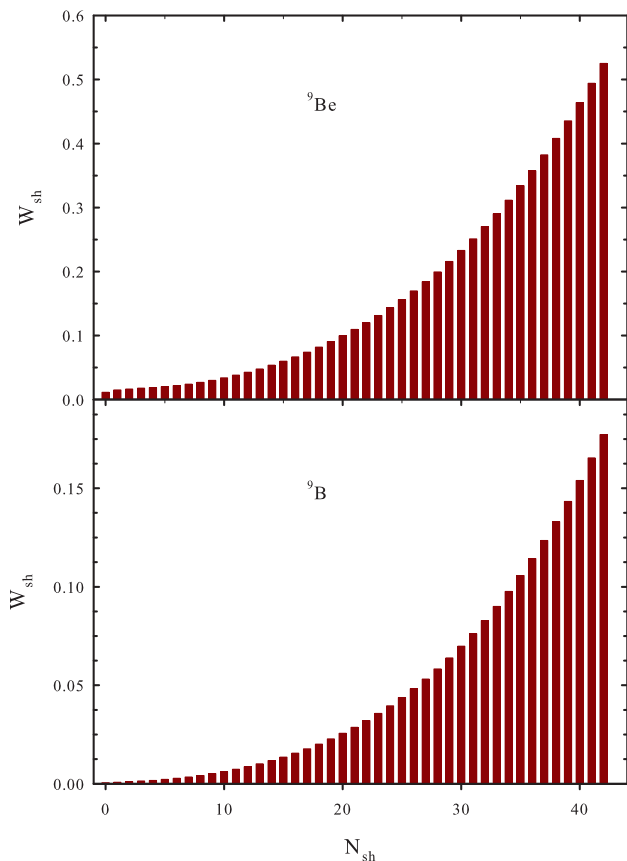


FIG. 8. Weights of different oscillator shells in wave functions of $1/2^+$ resonance states in ${}^9\text{Be}$ and ${}^9\text{B}$.

Such a behavior of resonance wave functions may explain why these resonances are difficult to detect by alternative methods.

It is important to note, that such shape of resonance wave function is observed not only for the $1/2^+$ resonance states in ${}^9\text{Be}$ and ${}^9\text{B}$ but also for the low-lying $1/2^+$ resonances in ${}^{11}\text{B}$ and ${}^{11}\text{C}$ as shown in Ref. [41]. These resonance states were considered as candidates for the Hoyle states in ${}^{11}\text{B}$ and ${}^{11}\text{C}$. They are narrower ($\Gamma = 12$ and $\Gamma = 163$ keV in $A = 11$ comparing to $\Gamma = 168$ and

$\Gamma = 477$ keV in $A = 9$) than the $1/2^+$ resonance states in ${}^9\text{Be}$ and ${}^9\text{B}$, however, the behavior of shell weights is very similar.

In Fig. 9 we show the weights W_{sh} for the narrow $3/2^-$ resonance state in ${}^9\text{B}$. This is a typical picture for very narrow resonance states in light nuclei. There are two main features of wave functions of narrow resonance states. First, the wave function is represented by the oscillator shells with small values of N_{sh} . Second, it has very large values of the weights W_{sh} for resonance states.

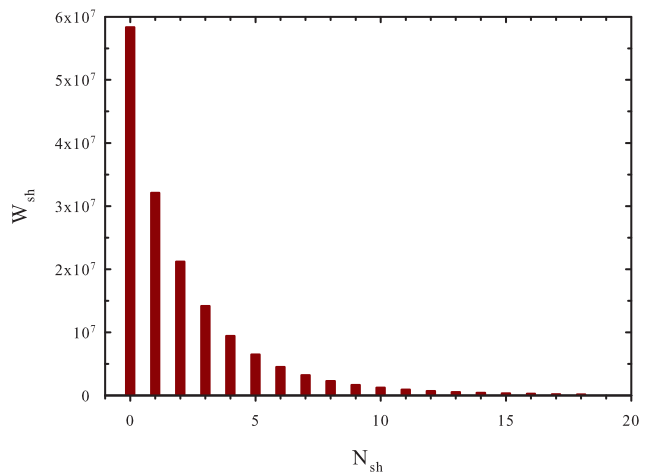


FIG. 9. Structure of wave function of the $3/2^-$ resonance state in ${}^9\text{B}$.

It should be stressed that all wave functions of continuous spectrum states are normalized by the standard condition

$$\langle \Psi_{E, J\pi} | \Psi_{\tilde{E}, J\pi} \rangle = \delta(k - \tilde{k}),$$

where

$$k = \sqrt{\frac{2mE}{\hbar^2}}, \quad \tilde{k} = \sqrt{\frac{2m\tilde{E}}{\hbar^2}}.$$

By analyzing the total and partial widths, we determine the dominant decay channels of a three-cluster resonance state. This analysis help us to shed some light on the nature of a resonance channel in many-channel systems. It can be performed for two different trees of the Jacobi vectors, which were denoted as $n+{}^8\text{Be}$ and ${}^4\text{He}+{}^5\text{He}$ in Ref. [2]. The $1/2^+$ resonance state in ${}^9\text{Be}$ and ${}^9\text{B}$ has only dominant channel. In the first tree, the resonance prefer to decay into the channel, where the relative orbital momentum of two alpha particles and the orbital momentum of valence neutron (with respect to the center of mass of two alpha particles) equal zero. Partial widths connected with that channel almost coincides with the total width. The same situation is observed in the second tree. There is also only one dominant channel

with zero values of partial orbital momenta. The first orbital momentum represents relative motion of neutron around first alpha particle and the second one represents relative motion of the second alpha particle with respect to the center of mass of the subsystem $\alpha + n$. These properties of the $1/2^+$ resonance states in ${}^9\text{Be}$ and ${}^9\text{B}$ are based on two important factors. The first factor is the dominant role of the channel with the hypermomentum $K = 0$ in wave function of the resonance state. The second factor is connected with the essential properties of the hyperspherical harmonics with $K = 0$. With this value of hypermomentum, we have got only one hyperspherical harmonic which is independent on choice of the Jacobi vector tree.

C. Resonances versus attraction

To shed some more light on structure of the $1/2^+$ states in ${}^9\text{Be}$ and ${}^9\text{B}$, we are going to increase attractive effective interaction in these nuclei by manipulating with the exchange parameter of nucleon-nucleon forces. By increasing the effective interaction in a many-channel system we expect to decrease energy and width of resonance states to persuade ourselves that the $1/2^+$ states in ${}^9\text{Be}$ and ${}^9\text{B}$ are resonance states. For virtual states such an increase of parameters or increase of attraction between clusters will lead to appearance of the corresponding bound states.

In Ref [27] such the procedure was used to study dependence of energy and width of the 0^+ resonance state in ${}^{12}\text{C}$ (well-known as the Hoyle state) on the exchange parameter u of the MP. It was shown that increasing of u (which results in increasing of the effective interaction in ${}^{12}\text{C}$) leads to decreasing of energy and width of the 0^+ resonance states, created by the interaction between three alpha particles. Here we use the same procedure and also the same nucleon-nucleon potential (namely the MP). The form of this potential allows to reduce significantly numeric calculations of parameters of $1/2^+$ resonance states as a function of u . We also believe that the same dependence of resonance parameters upon the exchange parameter of the nucleon-nucleon force can be obtained for the MHNP. In Figures 10 and 11 we display how energy and width of the $1/2^+$ resonance states in ${}^9\text{Be}$ and ${}^9\text{B}$ depend on the parameter u . Note that we start our calculations with $u=0.928$, which gives energy of the ${}^9\text{Be}$ ground state $E=-1.59$ MeV, and end up with $u=0.945$ which yields the bound state energy of ${}^9\text{Be}$ $E=-2.36$ MeV. This proves that we indeed increase the effective interaction (attraction) between clusters in ${}^9\text{Be}$ and ${}^9\text{B}$ by increasing the parameter u of the MP. As we see from Figure 10 that such a manipulation with the parameter u slightly decreases energy of the $1/2^+$ resonance state in ${}^9\text{B}$ and more strongly reduces (almost two times) energy of the resonance state in ${}^9\text{Be}$. Increasing of the effective attraction leads to more substantial changes of widths of $1/2^+$ resonance states. As we see from Fig-

ure 11 that the width of the $1/2^+$ resonance state in ${}^9\text{B}$ is diminished from 181 keV to 95 keV, while the width of the $1/2^+$ resonance state in ${}^9\text{Be}$ drops from 15 keV to 92 eV. Thus the $1/2^+$ resonance state in ${}^9\text{Be}$ became very a narrow resonance state which resides close to the $\alpha + \alpha + n$ threshold. However, the excitation energy of this state measured from the ${}^9\text{Be}$ ground states is increased from $E=1.80$ MeV ($u=0.928$) to $E=2.50$ MeV ($u=0.945$). It is interesting to note that a very narrow resonance state has a completely different wave function comparing to the wave function with starting values of the parameter $u=0.928$ or the wave function obtained with the MHNP. In Figure 12 we display weights of different oscillator shells in the wave function of a very narrow $1/2^+$ resonance state in ${}^9\text{Be}$. Comparing this Figure 12 with Figure 8, we see that the narrow resonance state has a large amplitude of wave function in the internal region and its wave function is represented by oscillator shells with small values of N_{sh} .

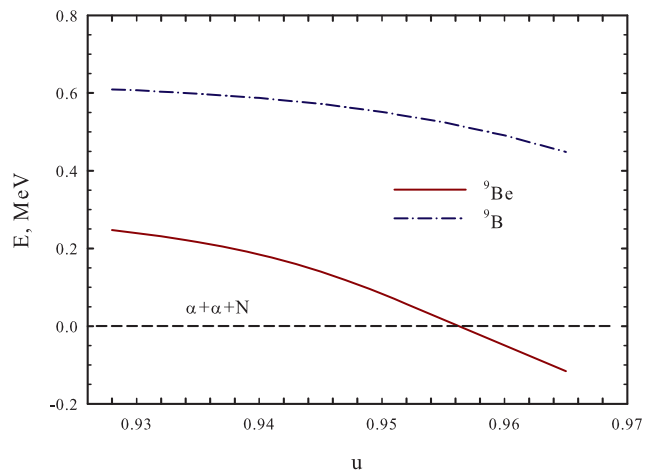


FIG. 10. Energy of $1/2^+$ resonance state in ${}^9\text{Be}$ and ${}^9\text{B}$ as a function of parameter u of the MP.

It is important to make the following comment. Because the binding energy of alpha clusters does not depend on the u -parameter, the threshold energy of $\alpha + \alpha + n(p)$ is independent of u . But the threshold energies of ${}^8\text{Be}+n(p)$ and ${}^5\text{He}({}^5\text{Li})+\alpha$ depend on u . The $1/2^+$ states in ${}^9\text{Be}$ and ${}^9\text{B}$ are calculated above the three-body $\alpha + \alpha + n(p)$ threshold but below the two-body threshold. Therefore, the calculated $1/2^+$ states are unbound for the three-body $\alpha + \alpha + n(p)$ threshold but bound state for the two-body threshold. The virtual state, which was observed, for instance, in Refs. [12, 13], is usually defined for the two-body threshold.

Results of the present section indicated that the $1/2^+$ states in ${}^9\text{Be}$ and ${}^9\text{B}$ are indeed resonance states. Besides, the analysis of dominant decay channels and wave functions leads us to the conclusion that the three-body effects, originated from nucleon-nucleon interaction and

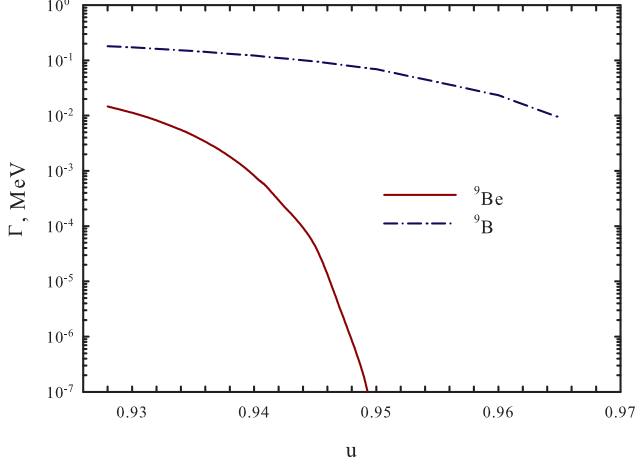


FIG. 11. Dependence of the width of the $1/2^+$ resonance state in ${}^9\text{Be}$ and ${}^9\text{B}$ on the parameter u of the MP.

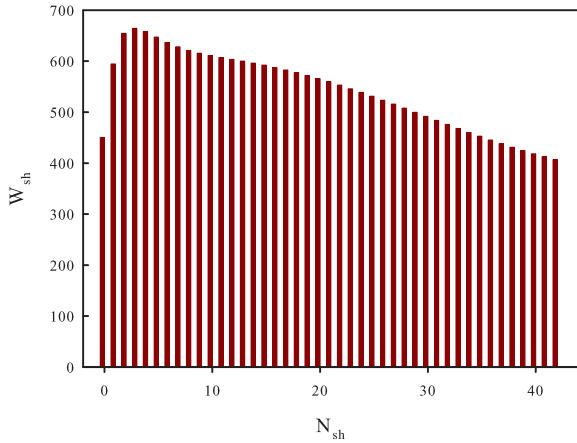


FIG. 12. Structure of wave function of the $1/2^+$ resonance states in ${}^9\text{Be}$ calculated with the MP and $u=0.945$.

the Coulomb potential between protons, and the Pauli principle plays very important role in formation of the $1/2^+$ resonance states in ${}^9\text{Be}$ and ${}^9\text{B}$.

V. EFFECTS OF COULOMB FORCES

Within the present model, differences in the position and of the total width of resonance states in mirror nuclei ${}^9\text{Be}$ and ${}^9\text{B}$ arise from the Coulomb interaction solely, which is more stronger in ${}^9\text{B}$ than in ${}^9\text{Be}$.

Effects of the Coulomb interaction on mirror or isobaric nuclei have been repeatedly investigated by many authors. Very often influence of the Coulomb potential on the spectrum of such nuclei is associated with the

Thomas-Erhman effect or shift (see, for instance, [42] and references therein), which is connected with the shift of energy of single particle levels in mirror nuclei due to the Coulomb interaction. By considering the mirror nuclei in the isotopic spin formalism, one can suggest two-fold effects of the Coulomb forces on parameters of resonance states. First, increasing of the Coulomb interaction leads to decreasing of the attractive effective interaction in each channel of a many-channel system. That may shift up energy of resonance states and may also increase width of resonance states. Second, the Coulomb interaction makes an effective barrier more wider, that may decrease both energy and width of resonance state. What scenario is realized in nuclei ${}^9\text{Be}$ and ${}^9\text{B}$ and how it depends on the total angular momentum J ?

A first effects of the Coulomb forces in the mirror nuclei ${}^9\text{Be}$ and ${}^9\text{B}$ can be seen in Figure 13 where spectrum of these nuclei is shown. Five dashed lines, connecting levels with the same total angular momentum J and parity π in ${}^9\text{Be}$ and ${}^9\text{B}$, show that Coulomb forces significantly shift up levels ($J^\pi = 3/2^-, 5/2^-, 5/2^+, 7/2^-$ and $9/2^-$) and four dashed lines indicate a moderate shift up of energy of resonance states ($J^\pi = 1/2^+, 3/2^-, 1/2^-$ and $3/2^+$) in ${}^9\text{B}$ comparing with correspondent states in ${}^9\text{Be}$.

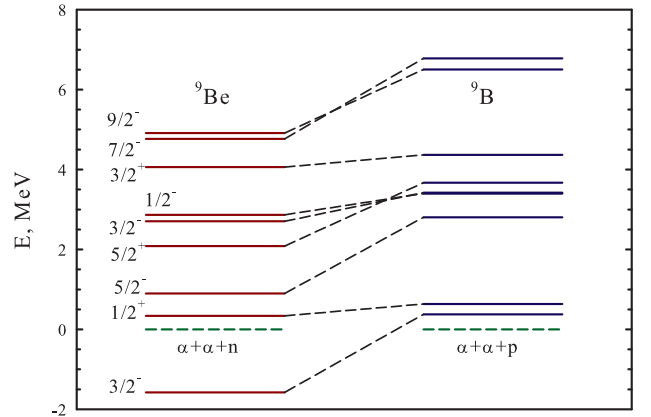


FIG. 13. Spectrum of bound and resonance states in ${}^9\text{Be}$ and ${}^9\text{B}$, calculated with the MHNP.

In Figure 14 we present how Coulomb forces affects both energy E and width Γ of resonance states. In this Figure resonance states of ${}^9\text{Be}$ are marked by triangle up, while resonance states of ${}^9\text{B}$ in the plane $E - \Gamma$ are indicated by triangle down. Dashed line in the Figure indicates situation when the width of a resonance state equals to its energy $\Gamma = E$. As one can see from Tables IV, V and from Figure 14 that energy of the resonance state of ${}^9\text{Be}$ with given total angular momentum J and parity π is lower than the analogue resonance state in ${}^9\text{B}$. All resonance states in ${}^9\text{Be}$ are more narrow than corresponding resonance states in ${}^9\text{B}$.

VI. HOYLE ANALOG STATES

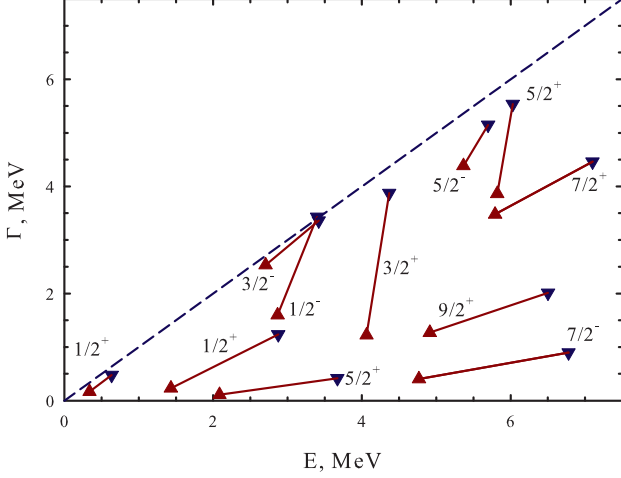


FIG. 14. Displacement of resonance states due to Coulomb interaction.

Results presented in Tables IV, V and Figures 13, 14 indicate that the first scenario is realized in mirror nuclei ${}^9\text{Be}$ and ${}^9\text{B}$. The Coulomb forces leads to the increasing both energy and width of resonance states. We can split all resonance states on three categories depending on effects of the Coulomb interaction. For this aim we calculate a "Coulomb shift angle"

$$\theta_C = \arctan \left(\frac{E({}^9\text{B}) - E({}^9\text{Be})}{\Gamma({}^9\text{B}) - \Gamma({}^9\text{Be})} \right)$$

for each pair of resonance states in ${}^9\text{Be}$ and ${}^9\text{B}$ with the given values of the total momentum J and parity π . The first category consists of resonance states with the Coulomb shift angle $40 \leq \theta_C \leq 50$ degrees. We call this category as a category with the moderate Coulomb effects. There are several resonance states when Coulomb forces increase energy and width in the same proportion. This leads to the case when the line connected analogue resonance states is parallel or almost parallel to the line $\Gamma = E$. These are $1/2^+$ and $3/2_2^-$ resonance states. The second category of resonance states consists of resonance states with the Coulomb shift angle $\theta_C < 37$ degrees and we call it as a category of weak Coulomb effects. In this case the Coulomb interaction changes strongly energy and weakly changes resonance width. This category includes $5/2_1^-$, $5/2_1^+$, $7/2^-$, $7/2^+$ and $9/2^+$ resonance states. The third category consists of resonance states with slightly changed energy but with strongly increased width. The Coulomb shift angle for this category $\theta_C > 66$ degrees. This category consists of four resonance states: $1/2^-$, $3/2^+$, $5/2_2^-$ and $5/2_2^+$.

Thus, the Coulomb interaction has week, moderate or strong influence on parameters of resonance states in mirror nuclei ${}^9\text{Be}$ and ${}^9\text{B}$.

We recall that the Hoyle state is a very narrow resonance state in ${}^{12}\text{C}$. It lies not far from the three-cluster threshold ($E = 0.38$ MeV) and has very small width $\Gamma = 8.5$ eV. One of the main features of the Hoyle resonance state that it is a very long-lived resonance state (according to nuclear scale). The Hoyle state is a dominant way for the nucleosynthesis of carbon in helium-burning red giant stars, which are rich of alpha particles. The present AM HHB model was successfully used in Ref. [27] to study a spectrum of bound and resonance states in ${}^{12}\text{C}$. It was obtained that the Hoyle state is generated by the triple collision of three alpha particles. (It should be stressed that the present model is accounted both for the sequential and simultaneous decay or excitation of a three-cluster resonance state. Technically it is very difficult to distinguish the sequential decay from simultaneous one. Thus, in our notion a term "the triple collision" stands for both types of processes.) These results of the present model encouraged us to search the Hoyle-analogue states in ${}^9\text{Be}$. There is a quest for the Hoyle-analogue states in light nuclei by different theoretical methods. Here, we are going to find in ${}^9\text{Be}$ the Hoyle-analogue state(s) by using the AM HHB model.

If we look at Table IV, we find that ${}^9\text{Be}$ has two resonance states ($1/2^+$ and $5/2^-$) which lie close to the three-cluster threshold $\alpha + \alpha + n$. However, the $1/2^+$ resonance state is not narrow one, as ratio Γ/E is large ($\Gamma/E \approx 0.5$). Meanwhile, the $5/2^-$ resonance state is indeed narrow resonance state because width is small $\Gamma = 23.6$ eV and besides ratio Γ/E is also very small: it equals $\Gamma/E \approx 2.63 \cdot 10^{-5}$ in our model and the experimental ratio is $\Gamma/E \approx 9.0 \cdot 10^{-4}$. One can compare this ratio with the experimental ratio $\Gamma/E \approx 2.24 \cdot 10^{-7}$ for the Hoyle state.

Our calculation indicates that the $5/2^-$ resonance state is the Hoyle-analogue state. This state has quite large half-life time, it could emit quadrupole gamma quanta and transit to the ground state of ${}^9\text{Be}$. This is one of possible ways for synthesis of ${}^9\text{Be}$. We assume, that in stars with large densities of alpha particles and neutrons this is a very plausible way of creating ${}^9\text{Be}$ nuclei.

The present model also indicates that the $1/2^+$ resonance state, being too wide or too short-lived one, has very small chance to participate in synthesis of ${}^9\text{Be}$.

Let us consider the structure of wave function of the $5/2^-$ resonance state in ${}^9\text{Be}$. In Figure 15 we demonstrate the weight W_{sh} of different shells in the wave function of the $5/2^-$ resonance state. It can be concluded from the Figure that the $5/2^-$ resonance state is a compact object, as it mainly represented by the oscillator shells with small number of N_{sh} . The structure of wave function of the $5/2^-$ resonance is similar to the structure of the ${}^9\text{Be}$ ground state wave function, which was displayed in Figure 3 in Ref. [2]. In both cases, the main contribution to wave functions of bound and resonance states comes from the oscillator shells $N_{sh} \leq 15$. Besides,

the wave function of the resonance state has a very large amplitude in the internal region ($W_{sh} \leq 10^6$). Such a behavior of the wave function of the $5/2^-$ resonance state in ${}^9\text{Be}$ is very similar to the behavior of the wave function of the Hoyle state in ${}^{12}\text{C}$ (see, for instance, Refs. [41, 43, 44]).

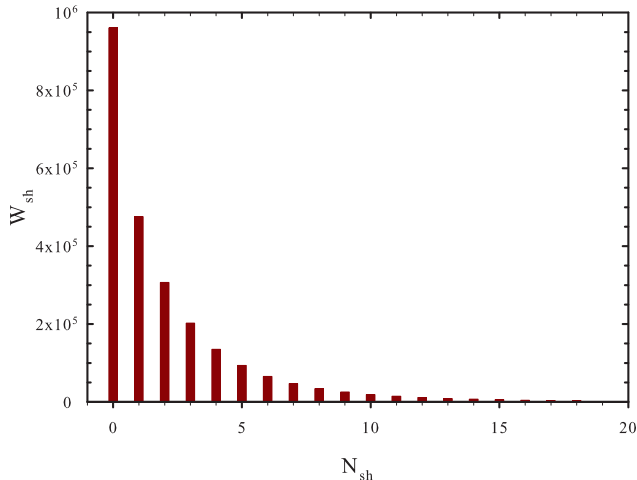


FIG. 15. Weights of different oscillator shells in the wave function of the $5/2^-$ resonance state in ${}^9\text{Be}$.

By comparing Figures 9 and 15 for resonance states $3/2^-$ in ${}^9\text{B}$ and $5/2^-$ in ${}^9\text{Be}$, respectively, we came to the conclusion that these figures represent the standard behavior of wave function for narrow resonance states. It means that the wave function of a “standard” resonance state has a very large amplitude in the internal region, this amplitude is much larger than the oscillating amplitude in the asymptotic regions. It also means that three clusters spend long time in the region, where inter-cluster distances are small and an interaction between them is strong.

Let us consider candidates to the Hoyle analog states in ${}^9\text{B}$. This nuclei, as was mentioned above, has no bound state and thus there is no way for creating of a stable state in the triple collision of two alpha particles and proton. However, one may consider the creation of a narrow resonance state in ${}^9\text{B}$, which can be then transformed into a bound state of ${}^9\text{Be}$ by emitting the beta particle or in combination of beta decay and gamma decay. This cascade of decay can be considered as an additional alternatively way for synthesis of ${}^9\text{Be}$ nucleus. As we see from Table V, there are two very narrow resonance states in ${}^9\text{B}$, they are the $3/2^-$ resonance state with a ratio $\Gamma/E \approx 2.8 \cdot 10^{-6}$ and the $5/2^-$ resonance state having a ration $\Gamma/E \approx 6 \cdot 10^{-3}$. The first resonance state, as was shown in Figure 9, is very compact and very narrow three-cluster state. The $5/2^-$ resonance state in ${}^9\text{B}$ is not so narrow as the $3/2^-$ state, however, it has a wave function with features which are typical for narrow resonance

TABLE X. Avarage distances $R_1 = R(N - \alpha\alpha)$ and $R_2 = R(\alpha - \alpha)$ (in fm) for few states of ${}^9\text{Be}$ and ${}^9\text{B}$.

${}^9\text{Be}$				
J^π	E	Γ	R_1	R_2
$3/2^-$	-1.574		3.71	3.38
$5/2^-$	0.897	$2.363 \cdot 10^{-5}$	4.75	3.52
$1/2^+$	0.338	0.168	14.02	7.37
${}^9\text{B}$				
J^π	E	Γ	R_1	R_2
$3/2^-$	0.378	$1.076 \cdot 10^{-6}$	3.96	3.50
$5/2^-$	2.805	0.017	5.01	3.87
$1/2^+$	0.636	0.477	14.33	7.44

state (see Figure 16).

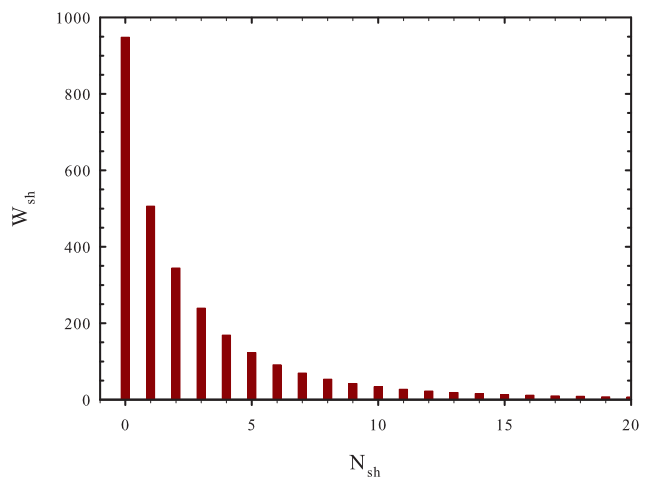


FIG. 16. Structure of wave function of the $5/2^-$ resonance state in ${}^9\text{B}$. Result is obtained with the MHNP.

Having calculated wave functions of a bound or resonance state, we can evaluate the shape of a triangle, connected the centers of mass of interacting clusters. In Table X we display average distances $R_2 = R(\alpha - \alpha)$ and $R_1 = R(N - \alpha\alpha)$ between clusters. The quantity $R(\alpha - \alpha)$ is an average distance between alpha particles, and $R_1 = R(n - \alpha\alpha)$ (or $R(p - \alpha\alpha)$) determines the average distance between the neutron (proton) and the center of mass of two alpha particles. It is important to note that to calculate average distances for resonance states we make use the internal part of wave functions, which we normalize to unity (see more detail in Refs. [2, 41] about definition of average distances between clusters).

Narrow resonance states, mentioned in Table X, have approximately the same size of a triangle as a bound state in ${}^9\text{Be}$. Meanwhile, the $1/2^+$ resonance states in ${}^9\text{Be}$ and ${}^9\text{B}$ are represented by a very large triangle. We assume that such dispersed (even in the internal region) resonance states have very small probability (comparing to the very narrow resonance states) to be transformed into a bound state.

VII. CONCLUSIONS

A three-cluster microscopic model was applied to studies of resonance states in mirror nuclei ${}^9\text{Be}$ and ${}^9\text{B}$. The model makes use of the hyperspherical harmonics to numerate channels of three-cluster continuum and simplify the method of solving of the Schrödinger equation for a many-particle and many-channel system. The MHNP modeled the nucleon-nucleon interaction. It was shown that the model with such an NN interaction provides a fairly good description of parameters of the known resonance states. This potential provides much better description of the spectrum of resonance states in ${}^9\text{Be}$ and ${}^9\text{B}$, than the MP, which was used in the previous paper [2]. It was shown that within the present model the excited $1/2^+$ states in ${}^9\text{Be}$ and ${}^9\text{B}$ are described as resonance states. It is also established that only one channel

with the hypermomentum $K = 0$ dominates in formation and decay of these $1/2^+$ resonance states. By analyzing effects of the Coulomb interaction, we discovered three groups of resonance states which reveal weak, medium and strong impact of the interaction on energy and width of resonance states. Our analysis leads us to the conclusion that the very narrow $5/2^-$ resonance state in ${}^9\text{Be}$ can be considered as the Hoyle-analogue state, and we assume that this state is a key resonance state for the synthesis of ${}^9\text{Be}$ in a triple collision of alpha particles and neutron in a stellar environment.

ACKNOWLEDGMENT

This work is partially supported by the Ministry of Education and Sciences of Republic of Kazakhstan, the Research Grant IPS 3106/GF4.

-
- [1] V. Vasilevsky, A. V. Nesterov, F. Arickx, and J. Broeckhove, Phys. Rev. C **63**, 034606 (16 pp) (2001), arXiv:nucl-th/0005045.
- [2] A. V. Nesterov, V. S. Vasilevsky, and T. P. Kovalenko, Phys. Atom. Nucl. **77**, 555 (2014).
- [3] A. Hasegawa and S. Nagata, Prog. Theor. Phys. **45**, 1786 (1971).
- [4] F. Tanabe, A. Tohsaki, and R. Tamagaki, Prog. Theor. Phys. **53**, 677 (1975).
- [5] P. Descouvemont, Phys. Rev. C **39**, 1557 (1989).
- [6] V. T. Voronchev, V. I. Kukulkin, V. N. Pomerantsev, K. D. Razikov, and G. G. Ryzhikh, Phys. Atom. Nucl. **57**, 1890 (1994).
- [7] K. Arai, Y. Ogawa, Y. Suzuki, and K. Varga, Phys. Rev. C **54**, 132 (1996), arXiv:nucl-th/9604009.
- [8] P. Descouvemont, Eur. Phys. J. A **12**, 413 (2001).
- [9] K. Arai, P. Descouvemont, D. Baye, and W. Catford, Phys. Rev. C **68**, 014310 (2003).
- [10] K. Arai, Nucl. Phys. A **738**, 342 (2004).
- [11] V. D. Efros and J. M. Bang, Eur. J. Phys. A **4**, 33 (1999), arXiv:nucl-th/9802077.
- [12] M. Odsuren, Y. Kikuchi, T. Myo, M. Aikawa, and K. Katō, Phys. Rev. C **92**, 014322 (2015), 1505.02353.
- [13] Y. Kikuchi, M. Odsuren, T. Myo, and K. Katō, Phys. Rev. C **93**, 054605 (2016), 1603.03861.
- [14] H. Akimune, M. Fujimura, M. Fujiwara, K. Hara, T. Ishikawa, T. Kawabata, H. Utsunomiya, T. Yamagata, K. Yamasaki, and M. Yosoi, Phys. Rev. C **64**, 041305 (2001).
- [15] O. Burda, P. von Neumann-Cosel, A. Richter, C. Forssén, and B. A. Brown, Phys. Rev. C **82**, 015808 (2010), 1006.2311.
- [16] R. Sherr and H. T. Fortune, Phys. Rev. C **70**, 054312 (2004).
- [17] H. Utsunomiya, Y. Yonezawa, H. Akimune, T. Yamagata, M. Ohta, M. Fujishiro, H. Toyokawa, and H. Ohgaki, Phys. Rev. C **63**, 018801 (2000).
- [18] F. C. Barker, Aust. J. Phys. **53**, 247 (2000).
- [19] J. P. Glickman, W. Bertozzi, T. N. Buti, S. Dixit, F. W. Hersman, C. E. Hyde-Wright, M. V. Hynes, R. W. Lourie, B. E. Norum, J. J. Kelly, et al., Phys. Rev. C **43**, 1740 (1991).
- [20] V. D. Efros, P. von Neumann-Cosel, and A. Richter, Phys. Rev. C **89**, 027301 (2014), 1308.1563.
- [21] M. A. Tiede, K. W. Kemper, N. R. Fletcher, D. Robson, D. D. Caussyn, S. J. Bennett, J. D. Brown, W. N. Catford, C. D. Jones, D. L. Watson, et al., Phys. Rev. C **52**, 1315 (1995).
- [22] K. Wildermuth and Y. Tang, *A unified theory of the nucleus* (Vieweg Verlag, Braunschweig, 1977).
- [23] R. I. Jibuti and N. B. Krupennikova, *Method of Hyperspherical Functions in quantum mechanics of few body systems. (In Russian)* (Micniereba, Tbilisi, 1984).
- [24] V. Vasilevsky, A. V. Nesterov, F. Arickx, and J. Broeckhove, Phys. Rev. C **63**, 034607 (7 pp) (2001), arXiv:nucl-th/0005047.
- [25] V. Vasilevsky, A. V. Nesterov, F. Arickx, and J. Broeckhove, Phys. Rev. C **63**, 064604 (8 pp) (2001).
- [26] M. Abramowitz and A. Stegun, *Handbook of Mathematical Functions* (Dover Publications, Inc., New-York, 1972).
- [27] V. Vasilevsky, F. Arickx, W. Vanroose, and J. Broeckhove, Phys. Rev. C **85**, 034318 (2012), 1109.1418.
- [28] D. R. Tilley, C. M. Cheves, J. L. Godwin, G. M. Hale, H. M. Hofmann, J. H. Kelley, C. G. Sheu, and H. R. Weller, Nucl. Phys. A **708**, 3 (2002).
- [29] D. R. Tilley, J. H. Kelley, J. L. Godwin, D. J. Millener, J. E. Purcell, C. G. Sheu, and H. R. Weller, Nucl. Phys. A **745**, 155 (2004).
- [30] J. Broeckhove, F. Arickx, P. Hellinckx, V. S. Vasilevsky, and A. V. Nesterov, J. Phys. G Nucl. Phys. **34**, 1955 (2007).
- [31] B. C. Pearce and B. F. Gibson, Phys. Rev. C **40**, 902 (1989).
- [32] A. Csótó, Phys. Rev. A **48**, 3390 (1993).
- [33] N. Tanaka, Y. Suzuki, K. Varga, and R. G. Lovas, Phys. Rev. C **59**, 1391 (1999).
- [34] G. Kuechler, A. Richter, and W. von Witsch, Z. Phys. A-Hadron Nucl. **326**, 447 (1987).

- [35] I. Mukha, M. Kavatsyuk, A. Algora, L. Batist, A. Blazhev, J. Döring, H. Grawe, M. Hellström, O. Kavatsyuk, R. Kirchner, et al., *Nucl. Phys. A* **758**, 647 (2005).
- [36] H. Utsunomiya, S. Katayama, I. Gheorghe, S. Imai, H. Yamaguchi, D. Kahl, Y. Sakaguchi, T. Shima, K. Takahisa, and S. Miyamoto, *Phys. Rev. C* **92**, 064323 (2015).
- [37] N. Arena, S. Cavallaro, G. Fazio, G. Giardina, A. Italiano, and F. Mezzanares, *Europhys. Lett.* **5**, 517 (1988).
- [38] T. D. Baldwin, W. N. Catford, D. Mahboub, C. N. Timis, N. I. Ashwood, N. M. Clarke, N. Curtis, V. Ziman, T. A. D. Brown, S. P. Fox, et al., *Phys. Rev. C* **86**, 034330 (2012).
- [39] R. I. Jibuti and R. Y. Kesperashvili, *Czech. J. Phys.* **30**, 1090 (1980).
- [40] M. Fabre de La Ripelle, *Few-Body Systems* **14**, 1 (1993).
- [41] V. S. Vasilevsky, *Ukr. J. Phys.* **58**, 544 (2013).
- [42] J. J. He and A. S. J. Murphy, *Eur. Phys. J. A* **34**, 315 (2007).
- [43] T. Neff and H. Feldmeier, *Int. J. Mod Phys. E* **17**, 2005 (2008).
- [44] T. Neff and H. Feldmeier, *Few-Body Syst.* **45**, 145 (2009).